Journal of Power Sources 196 (2011) 7488–7494

Contents lists available at ScienceDirect

Journal of Power Sources

journal homepage: www.elsevier.com/locate/jpowsour

A high-performance solid oxide fuel cell anode based on lanthanum strontium vanadate

Jong-Sung Park[a], Ian D. Hasson[b], Michael D. Gross[b], Chen Chen[a], J.M. Vohs[a], R.J. Gorte[a,*]

[a] Department of Chemical and Biomolecular Engineering, University of Pennsylvania, Philadelphia, PA, 19104, USA
[b] Department of Chemical Engineering, Bucknell University, Lewisburg, PA, 17837, USA

ARTICLE INFO

Article history:
Received 23 February 2011
Accepted 12 May 2011
Available online 19 May 2011

Keywords:
Fuel cells
Ceramic composite
Catalyst
Strontium vanadate
Composite anode
LSV

ABSTRACT

Ceramic composites were prepared by infiltration of $La_{0.7}Sr_{0.3}VO_{3.85}$ (LSV) into porous scaffolds of yttria-stabilized zirconia (YSZ) and tested for use as solid oxide fuel cell (SOFC) anodes. There was no evidence for solid-state reaction between LSV and YSZ at calcination temperatures up to 1273 K. For calcination at 973 K, LSV formed a continuous film over the YSZ. The LSV phase reduced easily upon heating in H_2 to 973 K, with the reduction forming pores in the LSV and greatly increasing its surface area. The electrodes showed high electronic conductivity after reduction, with a 10-vol% LSV–YSZ composite exhibiting a conductivity of 2 S cm^{-1} at 973 K. In the absence of an added catalyst, the LSV–YSZ electrodes showed relatively poor performance; however, an electrode impedance of approximately 0.1 Ω cm^2 was achieved at 973 K in humidified H_2 following addition of 0.5 vol% Pd and 2.8 vol% ceria The LSV–YSZ composites were stable in CH_4 but there was evidence for poisoning of the Pd catalyst by V following high-temperature oxidation.

1. Introduction

Solid oxide fuel cells (SOFC) have great potential as energy-conversion devices. Because the electrolytes are usually oxygen-ion conductors, SOFC can in principle operate on any combustible fuel with high efficiency and a low output of pollutants. At present, state-of-the-art SOFC anodes are composites of Ni and the electrolyte material. These ceramic–metal (cermet) composites exhibit excellent electrochemical and catalytic performance but are limited in their ability to operate on hydrocarbon fuels due to the tendency of Ni to catalyze the formation of carbon filaments [1–6]. For example, Ni-based anodes are able to operate on syngas (a mixture of CO and H_2) or methane if sufficient steam is co-fed with the Ni [7]; but operation on larger hydrocarbons is not practical under normal conditions [8]. Furthermore, even the best engineered Ni-based electrodes have only limited tolerance to oxidation during start-up and shut-down cycles due to the expansion that occurs when Ni forms NiO [9].

Electrodes based on electronically conductive oxides could solve some of the problems associated with Ni-based electrodes. Oxides do not catalyze the formation of filamentous carbon and the volumetric changes associated with oxidation and reduction are expected to be less than that for conversion between Ni and NiO. Unfortunately, the performance of ceramic fuel electrodes is usually very poor because of the following factors. First, it is difficult to achieve good conductivity with oxides under reducing conditions [10]. Second, the reactivity of most oxides with YSZ prevents one from using the high-temperature processing methods that give Ni cermets their nearly ideal interfacial structure with the electrolyte [11]. Third, compared to metals like Ni, oxides are very poor oxidation catalysts [12,13].

To minimize these problems, our groups have been focusing on the preparation of composite electrodes using infiltration methods [14–17]. This fabrication procedure involves first synthesizing a porous layer of the electrolyte that has been pre-sintered to the dense electrolyte, then infiltrating the catalytic and electronically conductive components into the porous scaffold [14]. With composites prepared by infiltration, the sintering temperature for the electrolyte component of the composite electrode can be much higher so as to establish better ion-conducting channels from the electrolyte into the electrode. Furthermore, the composites formed by infiltration do not have a random structure, so that sufficient conductivity can be achieved using lower loadings of the electronic conductor [18]. The non-random structure also causes the coefficients of thermal expansion (CTE) of the composite to be closer to that of the electrolyte scaffold than to the weighted average of the components [19,20]. The effects of expansion due to redox of the electronic conductor are minimized [17,21]. Finally, catalytic components can be added separately if required [22–24].

While we have been able to achieve very good performance with fuel electrodes based on infiltrated $La_{0.8}Sr_{0.2}Cr_{0.5}Mn_{0.5}O_3$ (LSCM)

* Corresponding author. Tel.: +1 215 898 4439; fax: +1 215 573 2093.
E-mail address: gorte@seas.upenn.edu (R.J. Gorte).

0378-7753/$ – see front matter © 2011 Elsevier B.V. All rights reserved.
doi:10.1016/j.jpowsour.2011.05.028

[22,23], $La_{0.3}Sr_{0.7}TiO_3$ (LST) [25] and $SrMoO_3$ [17] when a separate catalyst is added, each of these ceramic conductors has serious limitations. In the case of LSCM, the conductivity is only marginal; under reducing conditions at 973 K, the conductivity of bulk LSCM is less than 2 S cm^{-1} and composites formed by infiltration of 45-wt% LSCM in yttria-stabilized zirconia (YSZ) are a factor of 20 times lower. Ideally, the composite should have a conductivity of at least 1 S cm^{-1}. The conductivity of bulk LST is only marginally better under normal reduction conditions [26]. While bulk $SrMoO_3$ has a conductivity of nearly 1000 S cm^{-1} [17], $SrMoO_4$ is difficult to reduce and $SrMoO_3$–$SrMoO_4$ equilibrium data suggest that $SrMoO_4$ will be the stable phase under typical SOFC operating conditions [27].

Sr-doped $LaVO_3$ (LSV) is a particularly interesting material because its conductivity can be very high [28–30]. A thermodynamic investigation of the equilibrium between $LaVO_4$ and $LaVO_3$ indicated that the reduced phase will be stable at $P(O_2)$ below 10^{-18} atm at 973 K [31], which is similar to the equilibrium conditions for Ni. Although LSV has been used in SOFC fuel electrodes, conventional methods for preparing electrodes from this oxide have resulted in electrodes with only modest performance and only at temperatures well above 973 K [32–35]. Interestingly, this previous work has shown LSV to have a low reactivity with YSZ and good tolerance to sulfur [33,34].

In the present study, we set out to investigate the performance of SOFC anodes prepared by infiltration of LSV into YSZ scaffolds. We will demonstrate that the LSV–YSZ composites exhibit high electronic conductivities and good electrode performance when a separate oxidation catalyst is added to the composite.

2. Experimental

The electrochemical cells used in this study were prepared from tri-layer, YSZ wafers, in which an 80-μm dense electrolyte disc was sandwiched between two 40-μm porous YSZ layers. The diameter of the dense part of each wafer was 1 cm but the diameter of the porous regions was only 0.67 cm. The tri-layer wafers were fabricated by laminating three green tapes followed by calcination at 1773 K for 4 h. The tapes used in this study were cast using a slurry formulation based on organic solvents. The composition of the slurry and the procedures used to prepare the tapes are described elsewhere [36]. Porosity in the sintered layers was achieved by including synthetic graphite (300 mesh, Alfa Aesar) in the tapes used to prepare the porous YSZ layers. By comparing the apparent density of the porous YSZ to the bulk density of YSZ, the porosity of the layers made from tapes with graphite pore formers was determined to be 73 ± 1%.

To prepare composites of LSV and YSZ, we first prepared precursor solutions consisting of $La(NO_3)_3{\cdot}6H_2O$ (99.9%, Alfa Aesar), $Sr(NO_3)_2$ (99.9%, Alfa Aesar), NH_4VO_3 (99%, Alfa Aesar), and citric acid (one mole per mole of metal cations) dissolved in deionized water. The solutions were heated to 330 K and stirred for approximately 3 h until the solutions stopped bubbling. The precursor solutions were added to the porous YSZ by multiple infiltration and drying cycles to a final loading of 10-vol% LSV, then calcined at either 973 K or 1373 K for 1 h. Unless otherwise noted, the stoichiometry of the oxidized LSV was $(La_{0.7}Sr_{0.3})VO_{3.85}$. The LSCM–YSZ composites were prepared by infiltration with an aqueous solution of $La(NO_3)_3{\cdot}6H_2O$, $Sr(NO_3)_2$, $Cr(NO_3)_3{\cdot}9H_2O$ (Acros Organics, 99%), $Mn(NO_3)_2{\cdot}6H_2O$ (Alfa Aesar, 99.98%), and citric acid to a loading of 20-vol% LSCM, followed by calcination to 1473 K for 4 h, as described elsewhere [23]. $La_{0.8}Sr_{0.2}FeO_3$ (LSF)–YSZ electrodes used in this study were fabricated by infiltrating the porous YSZ opposite the anode layer to a loading of 20-vol% LSF, then calcined at 1123 K for 4 h. The details of this procedure are described elsewhere [37,38]. The anode composites were prepared before the LSF–YSZ cathodes in all cases except for when the LSV–YSZ composites were calcined to only 973 K.

As a final step in cell preparation, CeO_2 (added as 1 M $Ce(NO_3)_3$, Alfa Aesar, 99.5%) and Pd (0.45 M tetraammine palladium(II) nitrate solution, Alfa Aesar, 99.9%) were added to the anode composites to enhance catalytic activity [22]. Each solution was infiltrated twice and the volume % of ceria and Pd were calculated based on the residual pore volumes remaining after adding either LSV or LSCM. The calculated electrode volume fractions in the LSV–YSZ composites were 2.8-vol% CeO_2 and 0.50-vol% Pd, while the corresponding volume fractions in the LSCM–YSZ composites were 2.4 vol% and 0.42 vol%, respectively. Following the addition of the catalytic components, the cells were calcined to 773 K to decompose the nitrate ions, unless otherwise indicated. Some experiments were conducted on cells that were calcined to 973 K following the addition of the catalyst.

For fuel-cell testing, cells were attached to alumina tube using a ceramic adhesive (Ceramabond 552, Aremco). Ag paste (lot no. 1120912, SPI supplies) and Ag wire were used for current collection at both the anode and cathode. *V–i* polarization curves and impedance spectra were measured using a Gamry Instruments potentiostat with the cathode exposed to air and the anode exposed to humidified (3% H_2O) H_2 or CH_4. Impedance spectra were measured at −0.1 V bias voltage in the frequency range from 100 kHz to 0.01 Hz, with a 20-mV AC perturbation.

LSV–YSZ and LSCM–YSZ composites were also fabricated from YSZ porous slabs prepared from the same slurry used in tape casting the porous layers. The dimensions of the slabs used in the conductivity and BET-isotherm measurements were 1 mm × 1 mm × 10 mm and 0.5 cm × 0.5 cm × 1.8 cm, respectively. The conductivities were determined using 4-probe, DC measurements in humidified (3% H_2O) H_2. The BET surface areas were obtained using a Tristar II 3020 surface area analyzer (Micromeritics) using Kr adsorption at 78 K.

Thermogravimetric analysis (SDT Q600, TA Instruments) was used to investigate the reduction of LSV in 4% H_2/Ar and oxidation in air. A temperature ramp of 5 K min^{-1} from room temperature to 973 K and a gas flow rate of 50 mL min^{-1} was used for both oxidation and reduction experiments. The weight of the powder sample was ∼200 mg. The physical properties of LSV–YSZ composites were also investigated using X-ray diffraction (XRD) and scanning electron microscopy (SEM).

3. Results and discussion

In order to demonstrate that infiltration produced the proper phases, we examined the XRD patterns of various samples. Fig. 1a shows the pattern for the bulk powder having the stoichiometry $(La_{0.7}Sr_{0.3})VO_{3.85}$ after calcination in air at 973 K. The pattern is consistent with that which would be expected for the monoclinic structure of $LaVO_4$, with relatively broad features due to small crystallite sizes. After reduction in humidified H_2 at 973 K for 5 h, the XRD pattern changed dramatically and became similar to that of $LaVO_3$ (JCPDS card No. 81-2436), which has an orthorhombic crystal structure. The major peaks in the pattern for the reduced LSV show splitting, indicative of a tetragonal structure, which is reasonable due to the presence of Sr. The XRD patterns in Fig. 1c and d were obtained for LSV–YSZ composites after calcination at 1273 K and 1373 K, respectively, and reduction at 973 K. The pattern for the sample calcined at 1273 K shows only peaks associated with YSZ and the reduced LSV phase. The sample calcined at 1373 K contains additional small peaks at 28.2° and 31.8° 2θ, which are due to $La_2Zr_2O_7$ and possibly $Sr_3V_2O_8$, respectively, showing that some solid-state reaction had occurred.

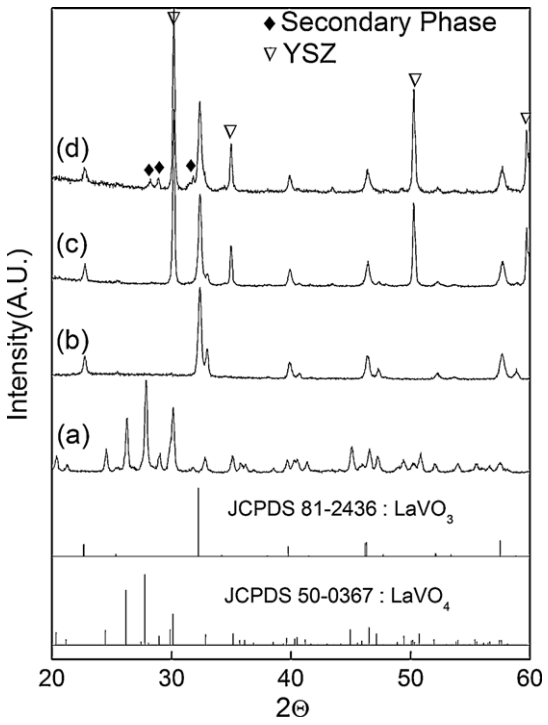

Fig. 1. XRD patterns of (a) $(La_{0.7}Sr_{0.3})VO_{3.85}$ synthesized at 973 K in air; (b) LSV after reduction at 973 K for 5 h in H_2. LSV–YSZ composite fabricated at (c) 1273 K and (d) 1373 K, followed by reduction at 973 K for 5 h in H_2.

TGA measurements were performed on LSV powder to determine the extent to which the sample is reduced at 973 K and provide a qualitative estimate of ease with which the LSV is reduced. The results are shown in Fig. 2. The reversible, 5.7% weight change upon oxidation and reduction corresponds to a change in the oxygen stoichiometry of 0.9 (i.e., a change from $(La_{0.7}Sr_{0.3})VO_{3.85}$ in the oxidized state to $(La_{0.7}Sr_{0.3})VO_{2.94}$), which is close to the expected extent of reduction. Reduction in 4% H_2–96% Ar began below 873 K and was nearly complete by 973 K. It is likely that the reduction was partially limited by the rate at which H_2 was supplied to the sample. Oxidation of the reduced LSV began at a much lower temperature, 573 K.

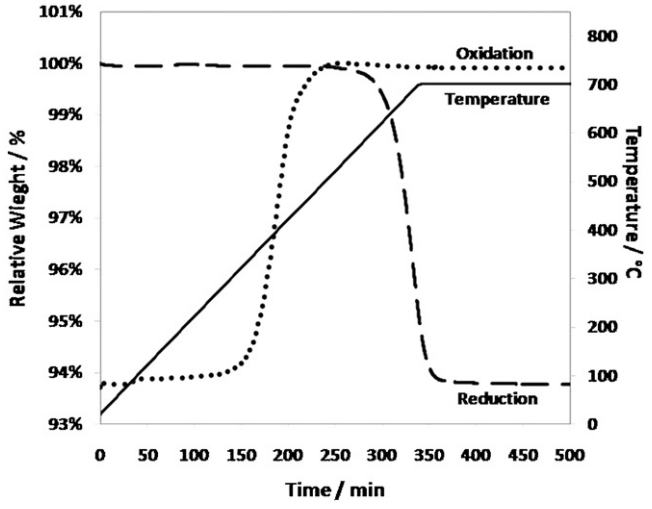

Fig. 2. TGA curves for the reduction of $La_{0.7}Sr_{0.3}VO_{3.85}$ in 4% H_2/Ar and oxidation of $La_{0.7}Sr_{0.3}VO_{2.85}$ in air.

Table 1
Specific surface areas of LSV–YSZ composites fabricated at 973 K or 1373 K, before and after reduction.

Fabrication temp. (K)	Surface area ($m^2\ g^{-1}$)	
	Before reduction	After reduction
973	0.13	1.14
1373	0.14	0.68

SEM micrographs of the LSV–YSZ composites calcined at 973 K and 1373 K, before and after reduction at 973 K, are shown in Fig. 3. Fig. 3a shows the YSZ scaffold before adding LSV. The scaffold has a "sponge-like" character, with characteristic pore dimensions between 1 and 3 μm. Following the addition of 10-vol% LSV and calcination at 973 K, the entire scaffold appears to be coated with a uniform, featureless film, as shown in Fig. 3b. Upon reduction at 973 K, Fig. 3c shows that cracks have formed in the LSV film. As shown in Fig. 3d, calcination to 1373 K caused the LSV film to break up into irregular-shaped features that no longer cover the entire YSZ surface. After reduction, Fig. 3e, small cracks again appear in the LSV structures.

The changes observed in the LSV following reduction are similar to what has been observed previously for LSCM in YSZ [39]. In that case, it was argued that these cracks were critical for exposing the YSZ and creating a long three-phase boundary (TPB). In order to better quantify the changes that occurred in the LSV layers upon reduction, the surface areas of the LSV–YSZ composites were measured using BET isotherms. Following calcination at 973 K, the LSV–YSZ composite had a surface area of 0.13 $m^2\ g^{-1}$ and this increased to 1.14 $m^2\ g^{-1}$ after reduction in H_2 at 973 K for 5 h. Following calcination at 1373 K, the increase in surface area with reduction, from 0.14 $m^2\ g^{-1}$ to 0.68 $m^2\ g^{-1}$, was less dramatic. These data are summarized in Table 1.

The electrical conductivities of LSV–YSZ composites, with 10-vol% LSV calcined at 973 K, and LSCM–YSZ composites, with 20-vol% LSCM, are shown in Fig. 4 as a function of temperature in humidified H_2. In a previous study of infiltrated, LSCM–YSZ composites with similar LSCM loadings [23], the electrical conductivities were slightly higher, near 0.1 S cm^{-1} at 973 K compared to 0.04 S cm^{-1} in this study, but showed a similar increase with increasing temperature. The difference between these and the previous LSCM–YSZ results is likely due to the fact that the YSZ scaffold used in the present work has a higher porosity, 73% compared to ~65%. More important is the fact that LSV–YSZ composite has a much higher conductivity, >2 S cm^{-1} at 973 K, even with only 10-vol% loading in the high-porosity YSZ scaffold. Based on the previous work of Hui and Petric [29], the conductivity of bulk $La_{0.7}Sr_{0.3}VO_{3-\delta}$ is approximately 100 S cm^{-1} at 1073 K under reducing conditions, so that the high conductivities we observe for the LSV–YSZ composites are reasonable. The conductivity of the LSV–YSZ composite was found to decrease slightly with increasing temperature.

Similar to what was found with SOFC anodes made with LSCM–YSZ composites [22,23], it is necessary to add a catalyst in order to achieve high performance with LSV–YSZ composites. This is shown in Fig. 5. In Fig. 5a, *V–i* polarization curves are shown for three cells operating at 973 K with humidified H_2 flowing over the anodes. Two of these cells had anodes with 10-vol% LSV, calcined at 973 K; but catalysts, Pd and ceria, were added to only one. The third cell had an anode with 20-vol% LSCM and a Pd/ceria catalyst. All three cells had identical LSF–YSZ cathodes and 80-μm thick electrolytes. The effect of adding the catalyst to the anodes made from LSV–YSZ was dramatic. While both cells exhibited the proper open-circuit voltage (OCV), 1.1 V, addition of the catalyst increased the maximum power density from 90 mW cm^{-2} to 470 mW cm^{-2}. Even with the Pd/ceria catalyst, the cell with the LSCM–YSZ anode

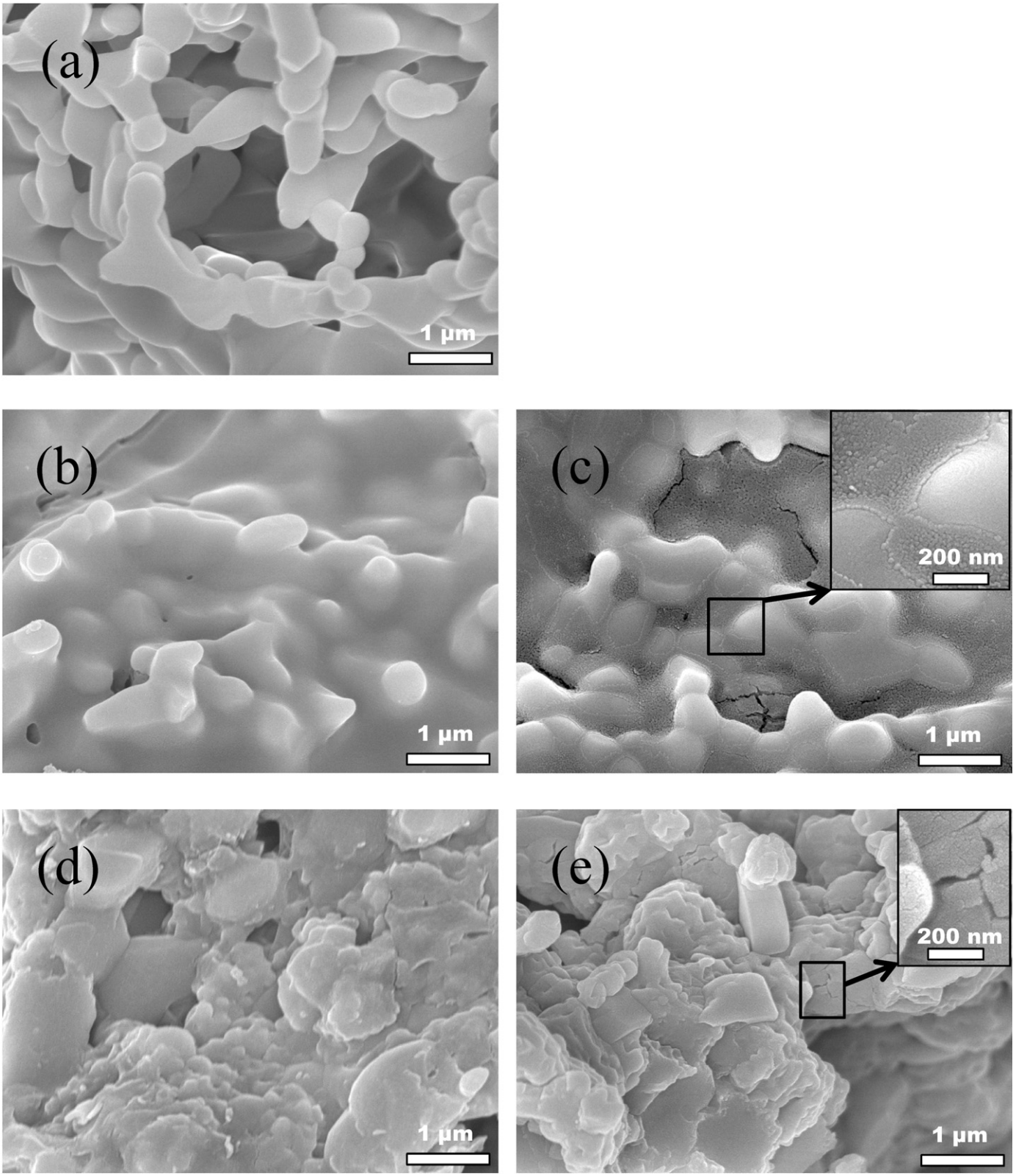

Fig. 3. SEM images of (a) the initial YSZ scaffold. The LSV–YSZ composite calcined at 973 K (b) before and (c) after reduction. The LSV–YSZ composite calcined at 1373 K (d) before and (e) after reduction.

performed slightly worse than the LSV–YSZ cell, showing a maximum power density of only 370 mW cm^{-2}.

The impedance spectra shown in Fig. 5b help to explain the differences between the three cells. First, the ohmic losses determined from the high-frequency intercepts with the real axis in the Nyquist plot were identical for the two LSV–YSZ cells, 0.43 Ω cm^2. Since the conductivity of YSZ at 973 K is reported to be 0.019 S cm^{-1} [40], this ohmic loss is consistent with that expected for the 80-μm electrolyte. Based on the measured conductivity of the LSV–YSZ composites in Fig. 4, 2 S cm^{-1}, the ohmic contribution

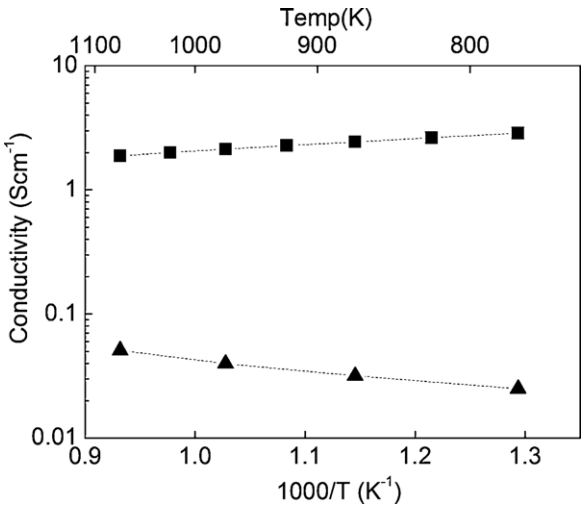

Fig. 4. Electrical conductivities of LSV–YSZ (■) and LSCM–YSZ composites (▲) measured in humidified (3% H_2O) H_2, using the DC 4-probes method.

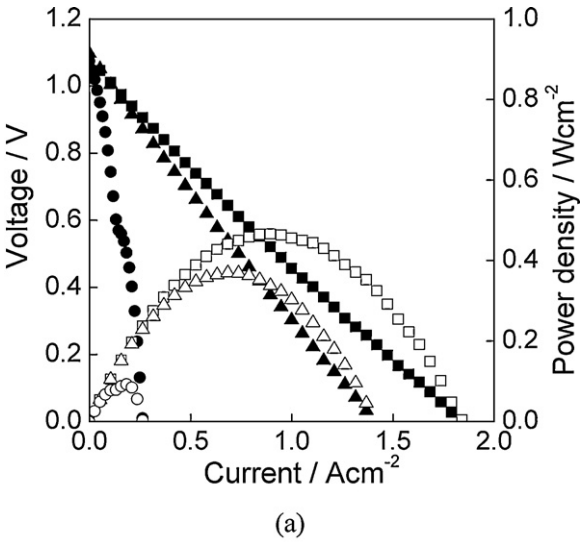

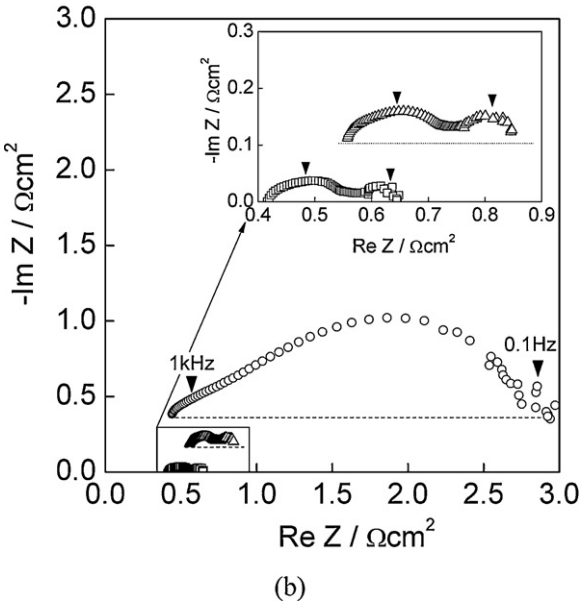

Fig. 5. (a) *V–i* polarization curves and (b) impedance spectra of cells at 973 K using LSV–YSZ anode with (■) and without (●) CeO_2 and Pd. Data for the LSCM–YSZ anode with CeO_2 and Pd (▲).

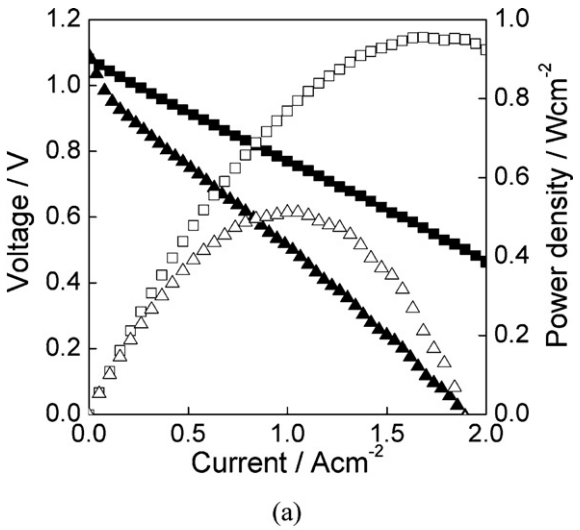

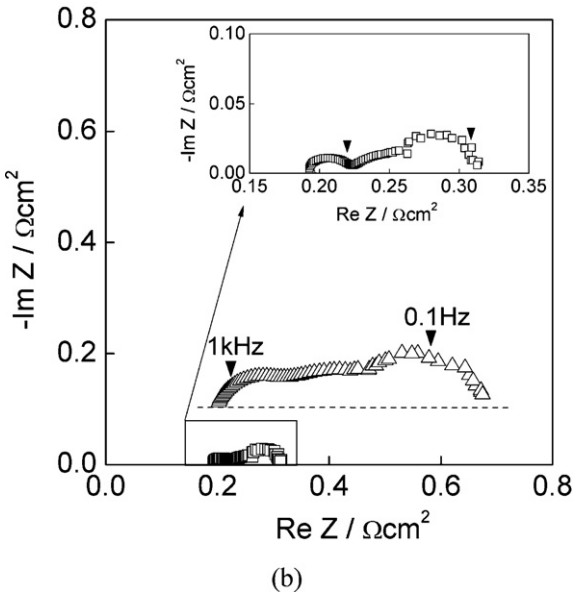

Fig. 6. (a) *V–i* polarization curves and (b) impedance spectra of cell having LSV–YSZ anode with CeO_2 and Pd in humidified (3% H_2O) H_2 (■) or CH_4 (▲) at 1073 K.

from the 40-μm anode is expected to be less than 0.002 Ω cm^2. The addition of the Pd/ceria catalyst caused a large decrease in the non-ohmic losses, from 2.5 Ω cm^2 for the cell without the catalyst to ~0.2 Ω cm^2 for the cell with the catalyst. This result is similar to what has been reported for anodes made from infiltrated LSCM [22,23] and LST [25], where the addition of a catalyst was also found to be critical for obtaining high performance. Given that the LSF–YSZ cathode likely contributes ~0.1 Ω cm^2 [37,38], the LSV–YSZ anode with the Pd/ceria catalyst must contribute ~0.1 Ω cm^2.

The impedance data in Fig. 5b also help to explain the lower performance of the LSCM–YSZ cell. While the non-ohmic losses in this cell were nearly identical, the ohmic losses were ~0.1 Ω cm^2 higher, as expected for a 40-μm electrode with a conductivity of 0.04 S cm^{-1}. This result points out the benefit of achieving higher electronic conductivity with the LSV–YSZ composite.

To determine the stability of LSV–YSZ composites in hydrocarbon fuels, we examined the performance of the cell with the Pd and ceria catalyst in methane. The *V–i* polarization curves and Cole–Cole plots for the cell operating at 1073 K in both humidified (3% H_2O) CH_4 and H_2 are shown in Fig. 6. The results are very similar to those obtained previously for a cell based on an LSCM–YSZ

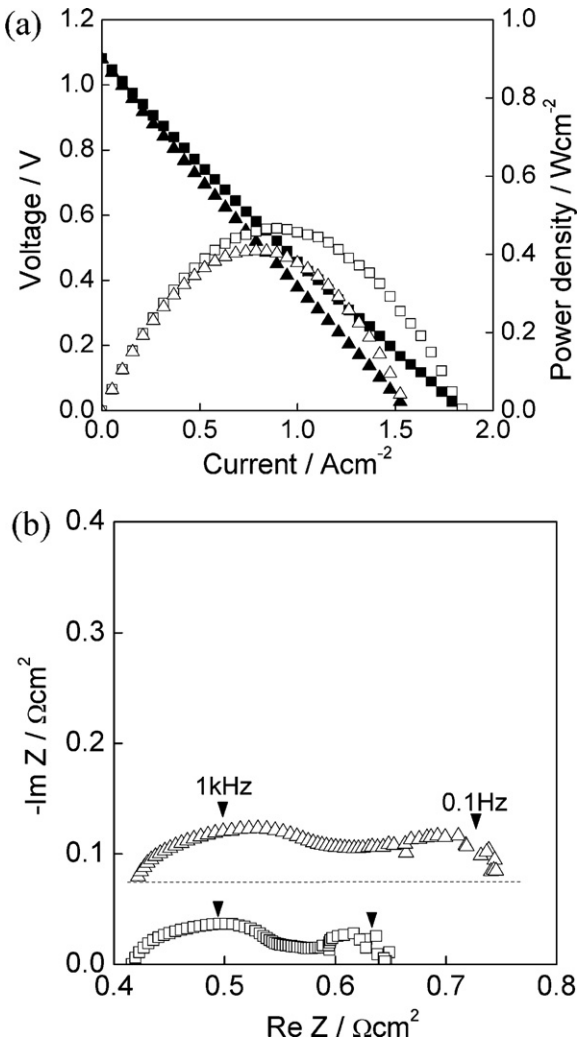

Fig. 7. (a) *V–i* polarization curves and (b) impedance spectra in humidified (3% H_2O) H_2 for cells having LSV fabricated at 973 K (■) or 1373 K (▲).

composite with Pd and ceria added [23]. The OCV was the same for both fuels, 1.1 V; but the maximum power density was significantly higher in H_2 than in CH_4, 960 mW cm^{-2} in H_2 compared to only 510 mW cm^{-2} in CH_4. While the *V–i* relationship was a straight line with H_2, there was noticeable curvature near open circuit with CH_4. The impedance data, measured at open circuit, show that ohmic losses were independent of fuel and ~0.2 Ω cm^2, but that the non-ohmic losses were significantly higher in CH_4, demonstrating that there must be catalytic limitations to breaking the C–H bonds in this molecule. We did not test long-term stability of these anodes in CH_4 because it is known that Pd will form carbon over time [41]; however, the electrodes were stable over the testing period of approximately a day, suggesting that the LSV is not affected by the methane.

The effect of LSV calcination temperature on the electrodes is shown in Fig. 7 through a comparison of fuel-cell performance in H_2 at 973 K in which the 10-vol% LSV was calcined to either 973 K or 1373 K. For the 1373-K cell, the LSF cathode was added after formation of LSV; in both cells, the Pd and ceria were added separately and calcined to only 773 K prior to cell testing. For both cells, the *V–i* relationship in Fig. 7a was a straight line, starting from the expected OCV of 1.1 V, although the 973-K cell exhibited a higher maximum power density of 470 mW cm^{-2} compared to 410 mW cm^{-2} for the 1373-K cell. The impedance data in Fig. 7b show that the ohmic losses were the same for both cells, ~0.42 Ω cm^2, and that the lower

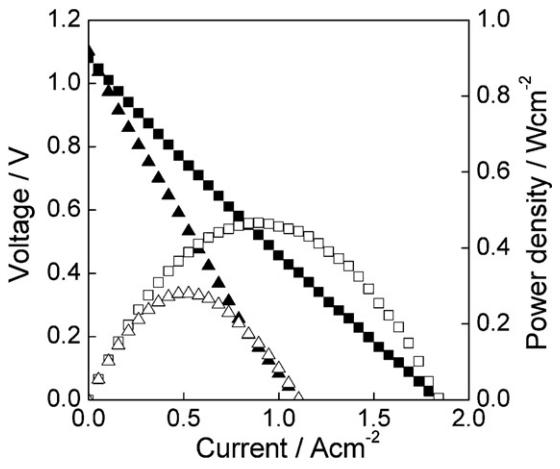

Fig. 8. *V–i* polarization curves in humidified (3% H_2O) H_2 for cells having LSV–YSZ anodes with Pd/ceria catalysts. Data are shown before (■) and after (▲) heating the composite to 973 K in air.

performance of the 1373-K cell is associated with an increase in the non-ohmic losses to 0.3 Ω cm^2. This result is important in that it indicates the impurity phases observed following calcination of the LSV–YSZ composite to 1373 K in Fig. 1 apparently do not significantly affect the conductivity within the electrode. The increase in the non-ohmic losses is likely caused by a decrease in the length of the TPB due to the change in the morphology of the infiltrated LSV, observed in Fig. 3.

We did observe a potential problem of LSV interacting with the Pd/ceria catalyst. When an LSV–YSZ cell with Pd and ceria was heated in air to 973 K, there was a significant decrease in performance, as shown by the *V–i* polarization curves in Fig. 8. Following calcination in air, the maximum power density in humidified H_2 at 973 K decreased from 470 mW cm^{-2} to 280 mW cm^{-2}. As expected, all of this change was associated with an increase in the non-ohmic cell losses. Similar treatments for electrodes made from LSCM–YSZ composites with Pd and ceria had no effect on cell performance. This is a potentially serious problem because the ability to oxidize the anode periodically is one of the advantages offered by anodes based on conducting ceramics.

From experiments conducted with LSCM–YSZ electrodes [22], it is known that the catalytic metal, Pd in this case, is the crucial catalytic component in anodes based on conducting ceramics. Since vanadium is a known poison in heterogeneous catalysis [42], it seems likely that the deterioration in performance of the LSV anodes is due to poisoning of the Pd catalyst by vanadium from the LSV. To test this hypothesis, we measured the performance of a series of similar fuel cells in which the vanadium stoichiometry of the LSV phase, $La_{0.7}Sr_{0.3}V_{1+\delta}O_{2.85}$, was varied. In each case, the LSV was calcined to 973 K prior to the addition of Pd and ceria and then calcined again to 973 K. The idea behind the experiments was that vanadium should be less able to migrate from the LSV phase if that phase is deficient in vanadium and more able to migrate if the vanadium is in excess.

The results from this experiment are shown in Table 2. Note that the ohmic losses were between 0.43 and 0.45 Ω cm^2, essentially unchanged by the vanadium stoichiometry or the increased catalyst calcination temperature. However, the maximum power densities were higher in the vanadium-deficient cell, 330 mW cm^{-2} compared to the vanadium-excess cell, 250 mW cm^{-2}. The variations in the power densities were matched by variations in the non-ohmic losses in each of the cells.

While the results in Table 2 are not entirely definitive in establishing that vanadium poisoning is responsible for the decrease in electrode performance following the exposure of the anode to

Table 2
Maximum power densities of the cells at 973 K in humidified H_2, with anode having 10 vol% LSV, together with Pd and ceria. In these experiments, the vanadium content of the LSV phase ($La_{0.7}Sr_{0.3}V_{1+\delta}O_{2.85}$) was varied and the cells were heated to 973 K in air to study the effect of interactions between the LSV phase and the Pd/ceria catalyst.

Non-stoichiometry of LSV	Power density ($mW\,cm^{-2}$)	Ohmic ASR ($\Omega\,cm^2$)	Non-ohmic ASR ($\Omega\,cm^2$)
$\delta = -0.05$	326	0.43	0.49
$\delta = 0$	280	0.45	0.61
$\delta = 0.05$	254	0.45	0.71

air at high temperatures, there are methods that could be used to minimize contact between the Pd catalyst and the LSV phase. For example, it has recently been demonstrated that Pd sintering in LSCM–YSZ electrodes could be dramatically reduced through the use of Pd/ceria, core–shell particles [43], in which Pd nanoparticles were surrounded by a thin shell of ceria, prepared using self-assembly methods [44]. It seems likely that the same oxide shell that mitigates Pd sintering may also minimize interactions between the metal and the LSV phase. This is obviously something that needs to be investigated further.

The most important conclusion to be taken from this work is the great similarities in the reported data for all of the ceramic SOFC anodes formed by infiltration [17,23,25]. Whether the infiltrated, conductive ceramic was LSCM, LST, $SrMoO_3$, or LSV, the data in each case suggest that the ceramic component simply provides electronic conductivity and that the catalytic function must be supplied by a second component which is added separately. There are obviously differences in the level of conductivity of the various ceramics and in their tendency to undergo solid-state reactions with the electrolyte phase. Interactions between the conductive ceramic and the electrolyte phase also seem to affect the morphology of the infiltrated component, which can in turn affect the length of the TPB. However, it appears that one can optimize each component of the electrode individually to maximize performance.

4. Conclusions

Ceramic composites with high electronic conductivity can be prepared by infiltration of $La_{0.7}Sr_{0.3}VO_{3.85}$ into porous YSZ. This material reduces easily and forms an effective three-phase boundary structure within the YSZ scaffold. The resulting composite has insufficient catalytic activity for optimal electrode performance but addition of a Pd/ceria catalyst produces electrodes with very low impedances in both H_2 and CH_4 fuels.

Acknowledgement

We thank the US Office of Naval Research for support for this work.

References

[1] S. McIntosh, R.J. Gorte, Chem. Rev. 104 (2004) 4845.
[2] H. Kim, C. Lu, W.L. Worrell, J.M. Vohs, R.J. Gorte, J. Electrochem. Soc. 149 (2002) A247.
[3] M.L. Toebes, J.H. Bitter, A.J. van Dillen, K.P. de Jong, Catal. Today 76 (2002) 33.
[4] C.W. Sun, U. Stimming, J. Power Sources 171 (2007) 247.
[5] S. Helveg, C. Lopez-Cartes, J. Sehested, P.L. Hansen, B.S. Clausen, J.R. Rostrup-Nielsen, F. Abild-Pedersen, J.K. Norskov, Nature 427 (2004) 426.
[6] K. Yamaji, H. Kishimoto, Y. Xiong, T. Horita, N. Sakai, M.E. Brito, H. Yokokawa, J. Power Sources 159 (2006) 885.
[7] S. Singhal, Ind. Ceram. 28 (2008) 53.
[8] M. Cimenti, J.M. Hill, Energies 2 (2009) 377.
[9] M. Cassidy, G. Lindsay, K. Kendall, J. Power Sources 61 (1996) 189–192.
[10] A. Atkinson, S. Barnett, R.J. Gorte, J.T.S. Irvine, A.J. Mcevoy, M. Mogensen, S.C. Singhal, J. Vohs, Nat. Mater. 3 (2004) 17–27.
[11] S. de Souza, S.J. Visco, L.C. De Jonghe, J. Electrochem. Soc. 144 (1997) L35.
[12] R.J. Gorte, J.M. Vohs, J. Catal. 216 (2003) 477.
[13] S. Park, R.J. Gorte, J.M. Vohs, Appl. Catal. A 200 (2000) 55.
[14] R.J. Gorte, S. Park, J.M. Vohs, C. Wang, Adv. Mater. 12 (2000) 1465.
[15] R. Craciun, R.J. Gorte, J.M. Vohs, C. Wang, W.L. Worrell, J. Electrochem. Soc. 146 (1999) 4019.
[16] M.D. Gross, K.M. Carver, M.A. Deighan, A. Schenkel, B.M. Smith, A.Z. Yee, J. Electrochem. Soc. 156 (2009) B540.
[17] B.H. Smith, M.D. Gross, Electrochem. Sol-State Lett. 14 (2011) B1.
[18] H. He, Y. Huang, J. Regal, M. Boaro, J.M. Vohs, R.J. Gorte, J. Am. Ceram. Soc. 87 (2004) 331.
[19] Y. Huang, K. Ahn, J.M. Vohs, R.J. Gorte, J. Electrochem. Soc. 151 (2004) A1592.
[20] J.M. Vohs, R.J. Gorte, Adv. Mater. 21 (2009) 943.
[21] A.N. Busawon, D. Sarantaridis, A. Atkinson, Electrochem. Solid-State Lett. 11 (2008) B186.
[22] G. Kim, S. Lee, J.Y. Shin, G. Corre, J.T.S. Irvine, J.M. Vohs, R.J. Gorte, Electrochem. Solid-State Lett. 12 (2009) B48.
[23] G. Kim, G. Corre, J.T.S. Irvine, J.M. Vohs, R.J. Gorte, Electrochem. Solid State Lett. 11 (2008) B16.
[24] M.D. Gross, J.M. Vohs, R.J. Gorte, J. Electrochem. Soc. 154 (2007) B694–B699.
[25] S. Lee, G. Kim, J.M. Vohs, R.J. Gorte, J. Electrochem. Soc. 155 (2008) B1179.
[26] Q.X. Fu, F. Tietz, D. Stover, J. Electrochem. Soc. 153 (2006) D74.
[27] I. Baldychev, A. Javadekar, D.J. Buttrey, J.M. Vohs, R.J. Gorte, Appl. Catal. A 394 (2011) 287.
[28] F. Inaba, T. Arima, T. Ishikawa, T. Katsufuji, Y. Tokura, Phys. Rev. B 52 (1995) R2221–R2224.
[29] Shiqiang Hui, Anthony Petric, Solid State Ionics 143 (2001) 275.
[30] Z. Cheng, S.W. Zha, L. Aguilar, M.L. Liu, Solid State Ionics 176 (2005) 1921.
[31] P.R. Shah, M.M. Khader, J.M. Vohs, R.J. Gorte, J. Phys. Chem. C 112 (2008) 2613.
[32] C. Peng, J.L. Luo, A.R. Sanger, K.T. Chuang, Chem. Mater. 22 (2010) 1032.
[33] Z. Cheng, S.W. Zha, L. Aguilar, D. Wang, J. Winnick, M.L. Liu, Electrochem. Solid State Lett. 9 (2006) A31.
[34] L. Aguilar, S.W. Zha, Z. Cheng, J. Winnick, M.L. Liu, J. Power Sources 135 (2004) 17.
[35] M. Ge, S.H. Chan, J. Electrochem. Soc. 156 (2009) B386.
[36] R. Küngas, J.-S. Kim, J.M. Vohs, R.J. Gorte, J. Am. Ceram. Soc., doi:10.1111/j.1551-2916.2010.04359.x.
[37] W. Wang, M.D. Gross, J.M. Vohs, R.J. Gorte, J. Electrochem. Soc. 154 (2007) B439.
[38] Y. Huang, J.M. Vohs, R.J. Gorte, J. Electrochem. Soc. 151 (2004) A646.
[39] G. Corre, G. Kim, M. Cassidy, J.M. Vohs, R.J. Gorte, J.T.S. Irvine, Chem. Mater. 21 (2009) 1077.
[40] K. Sasaki, J. Maier, Solid State Ionics 134 (2000) 303.
[41] J.-S. Kim, V.V. Nair, J.M. Vohs, R.J. Gorte, Scripta Mater. 65 (2011) 90.
[42] M.D.A Korn, D.S.S. do Santos, B. Welz, M.G.R. Vale, A.P. Teixeira, D.D. Lima, S.L.C. Ferreira, Talanta 73 (2007) 1.
[43] J.-S. Kim, Noah M. Cargnello, L. Wieder, R.J. Gorte, P. Fornasiero, J.M. Vohs, J. Electrochem. Soc. 158 (2011) B596.
[44] M. Cargnello, N.L. Wieder, T. Montini, R.J. Gorte, P. Fornasiero, J. Am. Chem. Soc. 132 (2010) 1402.